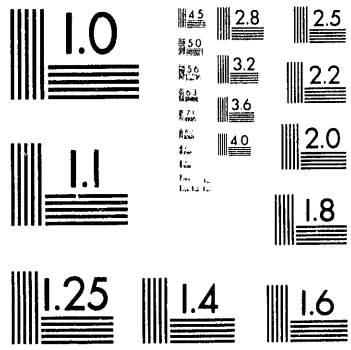
1.0
1.1
1.25
1.4
1.6
1.8
2.0
2.2
2.5
2.8
3.2
3.6
4.0
4.5
5.0

1 of 1

UCRL-JC-114892
PREPRINT

Baroclinic Mixing in HE Fireballs

A. L. Kuhl
R. E. Ferguson
F. Priolo
K.-Y. Chien
J. P. Collins

This paper was prepared for submittal to the
14th International Colloquium on the Dynamics of Explosions and Reactive Systems
Coimbra, Portugal
August 1-6, 1993

August 1993

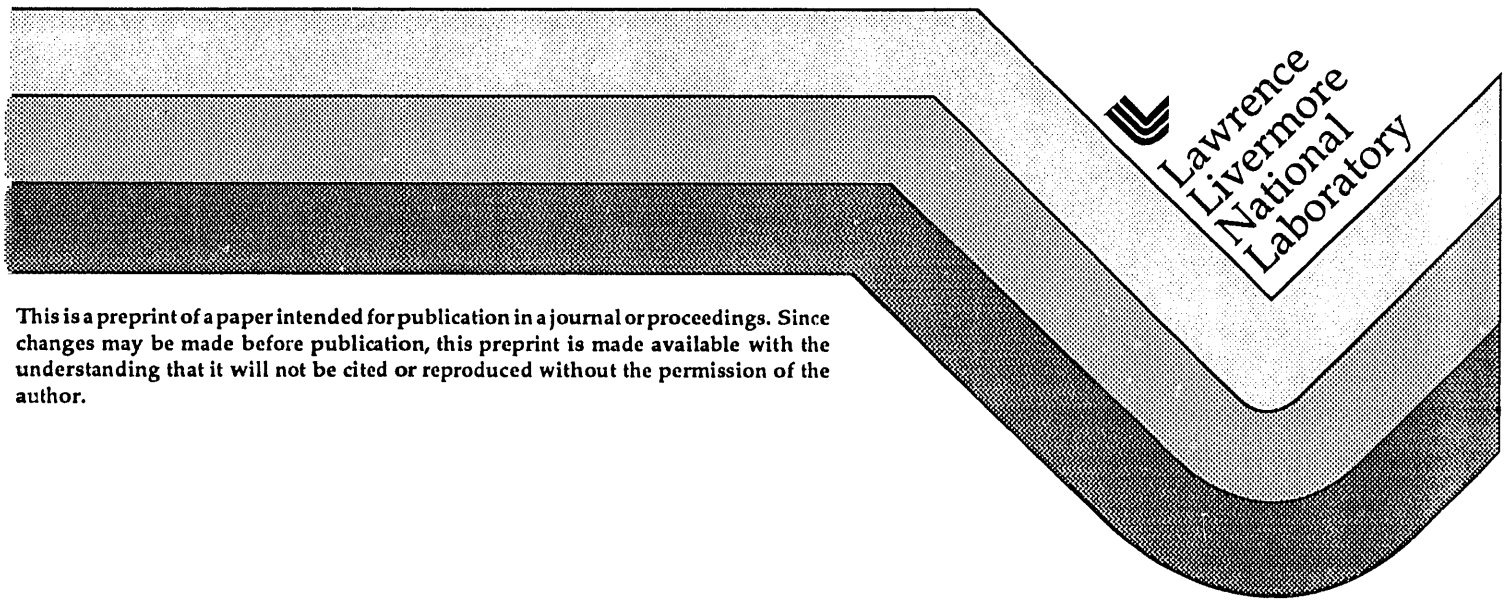

Baroclinic Mixing in HE Fireballs

A. L. Kuhl*
Lawrence Livermore National Laboratory
El Segundo, California

R.E. Ferguson, F. Priolo, K.-Y. Chien, and J.P. Collins
Naval Surface Warfare Center, White Oak Detachment
Silver Spring, Maryland

Abstract

Numerical simulations of the turbulent mixing in the fireball of an HE blast wave were performed with a second-order Godunov code. Adaptive mesh refinement was used to capture the convective mixing processes on the computational grid. The calculations revealed that the interface between the shock-compressed air and the dense detonation products was unstable. Vorticity was generated in that region by baroclinic effects (i.e., the vector cross-product of density gradients and pressure gradients). This caused the interface to roll-up into a turbulent mixing layer. Four phases of mixing were identified: (1) a strong blast wave phase, where the mixing region was swept outward by the shock-induced flow; (2) an implosion phase, that stretched the inner boundary of the mixing region back toward the origin; (3) a re-shocking phase, where the imploding shock expands back outward from the origin and re-energizes the mixing later by Richtmyer-Meshkov effects; and (4) an asymptotic mixing phase, where fine-scale structures are continually recreated by folding effects but the overall vorticity decays through a cascade process. The flowfield was azimuthally averaged to evaluate the mean-flow profiles and r.m.s. fluctuation profiles across the mixing layer. The mean kinetic energy rapidly approached zero as the blast wave decayed, but the fluctuating kinetic energy asymptotically approached a small constant value. This represents the rotational kinetic energy driven by the vorticity field, that continued to mix the fluid at late times. It was shown that the vorticity field corresponds to a function that fluctuates between plus and minus values–with a volume-averaged mean of zero. The amplitude of the vorticity fluctuations decayed a 1/t. The corresponding enstrophy increased linearly with time

* Work performed under the auspices of the U.S. Department of Energy by the Lawrence Livermore National Laboratory under Contract W-7405-ENG-48. Also sponsored by the Defense Nuclear Agency under DNA IACRO #92-824 and Work Unit 00001.

because of a cascade process for the mean-squared vorticity. This result is in agreement with the calculations of turbulent flow as reported by G.K. Batchelor.

Introduction

A fireball is created when a high explosives (HE) charge detonates. The fireball interface expands at a high velocity, initially around 9 km/s, which drives a strong blast wave into the surrounding atmosphere. The detonation products from solid explosives charges are typically very dense (~2.5 g/cm^3) compared to the shock-compressed air (~0.01 g/cm^3), hence the density ratio across the interface is very large (around 250). Such density interfaces are unstable to constant accelerations (e.g., Rayleigh-Taylor[1] instabilities), impulsive accelerations (as in Richtmyer[2]–Meshkov[3] instabilities), and misaligned pressure gradients (i.e., baroclinic effects). Small perturbations on the interface, arising either from granular irregularities on the charge surface or from molecular fluctuations, rapidly grow into a turbulent mixing region--as is quite evident from high-speed photography of explosions[4].

Turbulent mixing in fireballs is of scientific interest for a variety of reasons. First, mixing on a fireball interface can lead to afterburning for explosives that are not oxygen balanced (e.g., TNT). Afterburning can add considerable energy to the blast wave (as much as 30 percent) that is exceedingly difficult to calculate, since it depends on the turbulent mixing rate which is not known. On a more general note, turbulent fireballs provide an example of nonsteady compressible, turbulent mixing on density interfaces in spherical geometry. As will be shown here, such problems contain a wealth of fluid mechanic phenomena that are certainly worthy of detailed scientific investigation.

---

[1] Youngs, D.L. (1984) "Numerical Simulation of Turbulent Mixing by Rayleigh-Taylor Instability," *Physica*, 12D, pp. 32-44.

[2] Richtmyer, R.D. (1960) "Taylor Instability in Shock Acceleration of Compressible Fluids," *Comm. Pure Appl. Math*, 13, pp.297-319.

[3] Meshkov, E.E. 1960) "Instability of the Interface of Two Gases Accelerated by a Shock Wave," *Izv AN SSRE Mekhanika Zhidkosti i Gaza*, 4(15), pp. 151-157.

[4]

The first finite difference calculations of HE-driven blast waves (e.g., Brode[5]) were one-dimensional, hence mixing effects on the interface were neglected. More recently, a k–ε turbulence model which includes baroclinic effects (Issa[6]) has been added to blast wave calculations (Kuhl and Wright[7]) to estimate afterburning effects. However, the accuracy of any turbulence model is questionable for this case.

While others[8,9] have studied the growth of instabilities on planar density interfaces accelerated by shock waves, this paper investigates instabilities on a spherical density interface imbedded in an HE-driven blast wave. In particular, we shall study the dynamics of mixing in fireballs by following convective mixing processes on an adaptive mesh. This same methodology has been used to study spherical interface instabilities in high-altitude explosions[10] and implosions[11].

The formulation of the calculations is described in the next section. The results section presents: visualization of the mixing process, analyses of the mixing layer growth, mean and r.m.s. profiles across the layer, and evolution of the turbulent kinetic energy. This is followed by conclusions and recommendations for further work.

Formulation

The problem considered here is the blast wave created by the detonation of a spherical charge of PBX–9404, with an initial charge density of $\rho_0 = 1.84$ g/cm^3 and a corresponding detonation velocity of $W_{CJ} = 8.8$ km/s. For convenience, the charge

---

[5] Brode, H.L. (1959) "Blast Wave from a Spherical Charge, *Physics of Fluids*, 2(2), pp.217-229.

[6] Issa,

[7] **Kuhl, A.L. and Wright, M. (198)**

[8] Marcus, D.L., Puckett, E.G., Bell, J.B. and Saltzman, J. (1991) "Numerical Simulation of Accelerated Interfaces," UCRL-JC-108720.

[9] Ruppert, V. (1991) "Shock-Interface Interaction: Current Research on the Richtmyer-Meshkov Problem," *18th Int. Symp. on Shock waves*, Sendai, Japan (in press).

[10] Kuhl, A.L.,

[11] Klein, R.,

radius was assumed to be r_0 = 1.0 m; this results in a charge mass of 7,700 kg. The ambient gas was air at sea level conditions:

$$p_\infty = 1.01325 \text{ bars}; \ \rho_\infty = 1.2254 \times 10^{-3} \text{ g/cm}^3; \ e_\infty = 1.94 \times 10^9 \text{ erg/g};$$
$$a_\infty = 334 \text{ m/s}; \ \underline{U} = 0; \ \gamma = 1.41.$$

In order to focus on the convective mixing effects, a number of idealizing approximations were made. In particular, we assumed that: (1) the explosion is initially spherically symmetric; (2) The flow is inviscid (i.e., an infinite Reynolds number approximation, where molecular diffusion effects are neglected); (3) both the air and the detonation products are in local thermodynamic equilibrium; (4) the explosive is oxygen balanced (i.e., no afterburning), so the blast wave has constant energy; (5) buoyancy effects are neglected (in order to focus on baroclinic effects); (6) the flow is two-dimensional (2–D).

Based on the preceding assumptions, the flow is governed by the inviscid conservation laws of gas dynamics:

$$\frac{\delta}{\delta t}\rho + \nabla \cdot (\rho u) = 0 \qquad (1)$$

$$\frac{\delta}{\delta t}\rho u + \nabla \cdot (\rho u u) = -\nabla p \qquad (2)$$

$$\frac{\delta}{\delta t}\rho E + \nabla \cdot (\rho E u) = -\nabla \cdot (p u) \qquad (3)$$

Where u denotes the velocity and E represents the total energy E = e + 0.5 u•u. The pressure p is related to the density ρ and internal energy e by the equation of state. For air, it takes the well-known form:

$$p = (\gamma_e - 1)\rho e \qquad (4)$$

where the effective gamma $\gamma e = \gamma e(\rho 1 e)$ comes from the equilibrium air calculations of Gilmore[12]. A JWL equation of state was used for the detonation products:

$$p = A(1 - w\rho_0/\rho R_1)e^{-R_2\rho_0/\rho} + B(1 - w\rho_0/\rho R_2)e^{-R_2\rho_0/\rho} + (\gamma_d - 1)\rho e \qquad (5)$$

where according to Dobratz[13], A = 8.545 Mbars, B. = 0.2049 Mbars, R_1= 4.60, R_2 = 1.35 and γ_d = 1.25 for PBX-9404. In mixed cells, the pressure was defined as a mass-weighted average of the air and HE pressures.

In order to follow the mixing processes, an additional transport equation was used for concentration C:

$$\frac{\delta}{\delta t} C = (\mathbf{u} \cdot \nabla)C = 0 \qquad (6)$$

where C was initialized an C = 1 inside the charge ($r \leq r_0$) and C = 0 in the air ($r > r_0$).

The above set of equations (1,2,3 and 6) were integrated by means of a second-order Godunov algorithm[14,15]. Adaptive Mesh Refinement (AMR)[16] was used to follow the convective dynamics in the turbulent mixing region of the fireball.

In order to initialize the problem, we assumed that the chemical energy was released in the charge by an ideal Chapman–Jouguet (CJ) detonation wave[17]. Hence, the

---

[12] Gilmore, F.R. (1955) "Equilibruim Composition and Thermodynamic Properties of Air to 24000 K", RM-1543, Rand Corp., Santa Monica, CA.

[13] Dobratz, B. (1974) "Properties of Chemical Explosives and Explosive Simulants," UCRL-51319, Lawrence Livermore Laboratory, Livermore, CA.

[14] Colella, P. and Glaz, H.M. (1985) "Efficient Solution Algorithms for the Riemann Problem for Real Gases," *J. Comput. Phys* **59**, pp. 264-289.

[15] Colella, P. (1985) "A Direct Eulerian MUSCL Scheme for Gas Dynamics,"*SAIM J. Sci. Stat. Comput* **6**, pp. 104-117.

[16] Berger, M.J. and Colella, P. (1989) "Local Adaptive Mesh Refinement for Shock Hydrodynamics," *J. Comput Phys.* **82**, pp.64-84.

[17] Taylor, G.I. (1950)

flowfield in the charge was assumed to be that of a spherical CJ detonation[18] (see Figure 1) at the time when the wave reached the edge of the charge. The CJ parameters for a PBX–9404 charge are:

$$p_{CJ} = 370 \text{ kbars}; \rho_{CJ} = 2.485 \text{ g/cm}^3; e_{CJ} = 8.142 \times 10^{10} \text{ erg/g};$$
$$q_{CJ} = 5.543 \times 10^{10} \text{ erg/g}; u_{CJ} = 2.28 \text{ km/s}; \Gamma = 2.85$$

To desingularize the problem, and to qualitatively model the effects of HE grains on the charge surface, a linear gradient region was added to the outside of the charge to transition from the CJ state to the ambient state. In this region ($1.0 < r/r_0 < 1.10$), Gaussianly distributed random fluctuations were added to the density and energy profiles. This also served as a "white noise" seed for instabilities on the fireball interface.

An r-z cylindrical coordinate grid was used. To save computational time, only a quarter-space region of the spherical blast wave was actually calculated. Three levels of AMR grid refinement were used: a base grid, with a mesh size Δ_1 that extended to 100 r_0, was used to capture the shock; a transitional grid Δ_2; and fine grid Δ_3 to follow the mixing. The refinement strategy was based on following the detonation products region (i.e., where $C \leq 1$). To check for convergence, both a medium and a fine-grid calculation were performed. The mesh sizes are listed in Table 1.

Table 1

Case	Δ_1/r_0	Δ_2/r_0	Δ_3/r_0	CPU (hours) t = 62 ms	CPU (hours) t = 125 ms
1–medium zoning	0.90	0.15	0.0250	5	10
2–fine zoning	0.45	0.075	0.0125	30	–

The calculations were run out to a time of 62 ms or 125 ms (i.e., 2 to 4 times the positive phase duration of the blast wave). This took between 5 and 30 hours of CPU time on a Cray Y–MP computer, depending on grid resolution. The results are described in the next section.

---

[18] Kuhl, A.L. and Seizew, M.R. (1981) "TNT Explosions in a Hard Vacuum," *Gasdynamics of Detonations and Explosions, Progress in Astronautics and Aeronautics* **75** (ed. Bowen, et al.), AIAA, pp. 227-241.

Results

A. Flow Visualization

The next four figures present a sequence of frames that show the evolution of the blast wave in cross–section. In particular, density contours are used to visualize the shocks and mixing processes.

Figure 3 depicts the evolution of the flow during the strong blast wave phase. It shows that the detonation products rapidly expand, forming the main blast wave shock S and a secondary backward facing shock I that is swept outward by the blast wave flow. The fireball interface is located in the region between these two shocks.

The fireball interface is impulsively accelerated when the detonation wave reaches the edge of the charge. Thus, the interface is first subjected to impulsive accelerations that can lead to Richtmyer–Meshkov (RM) instabilities. As the fireball expands, it is decelerated by the shock-compressed air, and it is thus subjected to Rayleigh–Taylor (RT) instabilities. By a time of 2.4 ms, perturbations are clearly visible on the fireball interface (Figure 3c), which has expanded to about 8 charge radii.

Perturbations in this calculation originate from discretization errors resulting from the projection of the spherical interface onto the square r–z mesh. In the physical experiment, perturbations arise either from granular irregularities on the charge surface, or from molecular fluctuations. According to linear stability analysis, such perturbations will grow exponentially with time. Eventually they will be resolvable on the finite difference grid. Here we are interested in the late-time phase where there are strong interactions between various modes. This leads to a similarity spectrum of frequencies, and a concomitant loss of memory of the initial perturbations. Hence, for our purposes the cause of the initial perturbations is not particularly important.

By a time of 3.9 ms (or about 12 charge radii), the perturbations have evolved into mushroom–shaped structures that are characteristic of RM and RT-driven mixing layers (Figure 3d). These structures rapidly evolve into the nonlinear regime. By a time of 7.8 ms (or about 17.5 charge radii), they have generated new fine-scale structures through a nonlinear cascade process (figure 3f). Also, Kelvin–Helsnholtz (KH) instabilities develop due to shear flow along the bubble walls. Note that pressure gradients in the

blast wave are essentially radial. Perturbations on the fireball interface cause a misalignment of pressure and density gradients, that creates vorticity by the baroclinic mechanism:

$$\dot{\omega} = -\nabla(1/\rho) \times \nabla p \qquad (7)$$

This leads to a self–induced production of vorticity in the mixing region.

Figure 4 depicts the evolution of the flow during the implosion phase. At a time of about 12 ms, the secondary shock I falls into the negative phase of the blast wave, and starts propagation back toward the origin. It implodes at a time of about 24 ms. This draws the inner boundary of the mixing layer back toward the origin, thus greatly increasing the mixing width. During this phase, the flow exhibits many of features characteristic of imploding spherical shells[19] (e.g., elongated bubbles with KH structures on the bubble walls, perturbations on the imploding shock shape, etc.).

Figure 5 depicts the evolution of mixing in the fireball during the re-shocking phase. The implosion of shock I creates a second explosion shock S' which expands outward from the origin. This reshocks the mixing layer, and creates additional vorticity by baroclinic effects. The intensification of fine-scale structures is evident in this figure. At a time of about 60 ms, shock S' emerges from the fireball.

This leads to the asymptotic mixing phase, shown in Figure 6. It is characterized by a continued cascade process among the various vorticity scales, and a continued folding of the fireball interface. However, the mean radial expansion of the explosion has ceased, so the fireball size remains essentially constant.

B. Growth of the Mixing Layer

In order to study the growth of the mixing region, we found it useful to follow the evolution of certain mean• concentration lines. Three lines were selected :

---

[19] Batchelor, G.K., (1969) "Computation of the Energy Spectrum in Homogeneous Two-Dimensional, Supersonic Shear Layer," *Phys. of Fluids* (Supplement II), pp. II 233 to II 239.

• Mean concentrations will be defined in the next section.

1. The line $R_{0.9}(t)$ where $\overline{C} = 0.9$, which characterizes the inner boundary of the mixing region;
2. The line $R_{0.5}(t)$ where $\overline{C} = 0.5$, which represents the center of the mixing region; and
3. The line $R_{0.1}(t)$ where $\overline{C} = 0.1$, which characterizes the outer boundary of the mixing region.

These are depicted in the wave diagram for an HE-driven blast wave (Figure 7). Four distinct phases are evident:

1. A blast wave phase—where the mixing region is swept outward by the shock-induced flow;
2. An implosion phase—that stretched the inner boundary of the mixing region back toward the origin;
3. A re-shocking phase—that re-energizes the mixing layer by RM effects; and
4. An asymptotic mixing phase—where the fireball size remains essentially constant.

Let us define the mixing width by the relation:

$$\delta(t)/r_0 = [R_{0.1}(t) - R_{0.9}(t)]/r_0 \qquad (8)$$

The evolution of the mixing width is shown in Figure 8., During the blast wave phase, the mixing width grows linearly with time:

$$\delta(t)/r_0 = 0.396t \qquad (0 < t \leq 10 \text{ ms}) \qquad (9)$$
$$[t] = ms$$

At a velocity of 396 m/s. This is consistent with an impulsive acceleration of the fireball interface (i.e., a RM growth). During the implosion phase, the power-law exponent increases to a value of 1.44:

$$\delta/r_0 = 0.151t^{1.44} \qquad (10 \text{ ms} < t < 32 \text{ ms}) \qquad (10)$$

as a result of the inward stretching of the interface back toward the origin. Mixing occurs in a strong gradient of velocity (i.e., acceleration is not constant), so the quadratic growth associated with RT mixing is not achieved. During the re-shock phase, the mixing layer is compressed from $\delta/r_0 = 22$ to $\delta/r_0 = 16$ by the shock S'. During the asymptotic mixing phase, the mixing width is essentially constant : $\delta/r_0 \equiv 21$.

C. Azimuthal Averaging

In order to study the profiles in the mixing region, it is convenient to define an averaging procedure. In this problem, azimuthal averaging is most appropriate. The flow field variables Φ, were stored as a function of r, z, and t, that is $\Phi(r,z,t)$. One can define a polar-coordinate system in the r-z plane:

$$R = \sqrt{r^2 + z^2} \tag{11}$$

$$\theta = Tan^{-1}(z / r) \tag{12}$$

and convert the flowfield to the new variables, i.e., $\Phi(r,\theta,t)$. It is then possible to define an azimuthal of the flowfield by integrating over θ :

$$\overline{\Phi}(R,t) = \frac{2}{\pi}\int_0^{1/2} \Phi(R,\theta,t)\,d\theta \tag{13}$$

Given the average, one can then calculate root-mean-squared (r.m.s) fluctuations from the relation:

$$(\overline{\Phi'})^2 = \frac{2}{\pi}\int_0^{\pi/2} [\Phi(R,\theta,t) - \overline{\Phi}(R,t)]^2\,d\theta \tag{14}$$

and

$$\Phi = \sqrt{\overline{(\Phi')^2}} \tag{15}$$

D. Averaged Profiles

In order to check for similarity, the profiles were scaled with the mixing width δ:

$$\eta = (R - R_{0.5}) / \delta \tag{16}$$

In addition, the flowfield was nondimensionalized by the ambient atmosphere conditions, denoted by subscript ∞.

Figure 9 presents the azimuthally-averaged mean flow profiles across the mixing layer, during the blast wave phase. The mean concentration profiles tend to collapse to a single curve, independent of time. This provides indirect verification of the validity of the scaling procedure. The mean density profiles peak at the fireball interface at a value of $\sim 7\rho_\infty$ at early times, and then decay with time as that mass is spread over a larger and larger volume. Figure 9c indicates that there is a mean radial pressure gradient at the fireball interface during this phase. Figure 9d demonstrates that the azimuthal averaging procedure is adequate to produce smooth, well-behaved mean radial velocity profiles. Shock S and I are indicated on the figure. Of course, the magnitude of the velocity decays with time. The mean azimuthal velocities are typically less than 0.1 $\bar{u}$, and they oscillate about a mean value of zero--as one might expect. Figure 9f displays the azimuthally-averaged vorticity profiles across the layer. Perhaps one of the most significant results of this calculation is that the mean vorticity profiles decay with time, no doubt by means of cascade process. This is demonstrated definitively in figure 9f.

The corresponding r.m.s. profiles across the mixing layer are presented in Figure 10. Again note that the azimuthal-averaging procedure is adequate to give smooth, well-behaved profiles of the second moments of the flow variables. Again the concentration profiles collapse to a single curve, with peak fluctuation around 40 percent. Again, density fluctuations decay with time, as do the pressure fluctuations. The radial velocity fluctuation profiles are surprisingly smooth, and have a trimodal character, with peaks at the inner and outer edges of the layer and a peak at the center of the layer. Even the azimuthal velocity profiles are relatively smooth and well-behaved.

Figures 11 and 12 illustrate the evolution of the mixing layer by showing the profiles at the end of each of the four phases of the explosion. Again we find that the azimuthal-averaging procedure is adequate to give smooth, well-behaved profiles. The following profiles are approximately self-similar and independent of time: $\bar{c}$, $\bar{\rho}$, $\bar{p}$, c', ρ', p', u', and v'. Profiles exhibiting a marked decay are: the mean radial velocities $\bar{u}$ (due to blast wave decay), and vorticity $\bar{\omega}$ and ω' (as a consequence of a cascade process).

Mixing Properties

In order to check the global properties of the mixing processes, the various components of the kinetic energy were integrated over the mixing volume, in particular, the kinetic energy of the mean flow $\bar{\bar{k}}(t)$, the kinetic energy of the fluctuation flow k''(t), and the total kinetic energy K(t), were calculated from the following relations:

$$\bar{\bar{k}}(t) = \frac{3}{R_*^3}\int_0^{R_*}\frac{1}{2}\left[\bar{u}(R,t) + \bar{v}(R,t)^2\right]R^2\,dR \tag{17}$$

$$k''(t) = \frac{3}{R_*^3}\int_0^{R_*}\frac{1}{2}\left[u'(R,\theta,t)^2 + v'(R,t)^2\right]R^2\,dR \tag{18}$$

$$K(t) = \frac{3}{R_*^3}\frac{2}{\pi}\int_0^{R_*}\int_0^{\pi/2}\frac{1}{2}\left[u(R,\theta,t)^2 + v(R,\theta,t)^2\right]R^2\,d\theta\,dR \tag{19}$$

$$= \bar{\bar{k}}(t) + k''(t) \tag{20}$$

where a value of $R_* = 40\ r_0$ was used. The results are presented in Figure 13. It shows that the kinetic energy reaches a peak value of 6.5 x 10^8 $(cm/s)^2$ at t ≅ 6 ms, or about halfway through the blast wave phase. The mean kinetic energy then decays as the interface does work on the ambient atmosphere, and eventually approaches zero at late times. This is, of course, consistent with the finite energy of the explosion, which implies that the velocity field of the blast wave must eventually decay to zero. The fluctuating kinetic energy k'' reaches a peak value of 3.1 x 10^7 $(cm/s)^2$ (or about 10 percent of the instantaneous $\bar{\bar{k}}$) during the implosion phase. It decays slightly during the re-shock phase, and finally reaches a constant asymptotic value of k''_∞ = 2.2 x 10^7 $(cm/s)^2$; this is consistent with a residual fluctuating velocity of about 66 m/s that continues to mix the fluid in the fireball. The total kinetic energy, which represents the sum of the two components, tracks $\bar{\bar{k}}$ at early times and asymptotically approaches k'' at late times.

The fluctuating kinetic energy corresponds to the rotational energy of mixing induced by the vorticity distribution. The persistence of fluctuating kinetic energy at late times may be explained by considering the mechanical energy equation:

$$\frac{d}{dt}K = -\overline{\overline{u \bullet (\nabla p)/\rho}} + \nu \overline{\overline{u \bullet (\nabla^2 u)}} \qquad (21)$$
$$= -\overline{\overline{u \bullet (\nabla p)/\rho}} + \nu \overline{\overline{\omega^2}}$$

where the overbars denote averaging over the computational volume. The pressure gradients rapidly disappear and can no longer influence the kinetic energy. Since the present calculations are inviscid, shear work cannot affect the kinetic energy. Hence, conservation of mechanical energy implies that the rotational kinetic energy approaches a constant for inviscid blast waves. In the present calculations, the asymptotic value of this constant is $K_\infty = 2.3 \times 10^7$ (cm/s)^2 — or about 3.5 percent of its peak value at early times. From a numerical point of view, this persistence of fluctuating kinetic energy demonstrates that Godunov-AMR algorithm is non-dissipative. From a physical point of view, Equation (21) proves that viscosity is required to dissipate. Since the velocity or kinetic energy fluctuations are driven by the vorticity field, it is useful to consider the global properties of the vorticity, namely:

$$\overline{\overline{\omega(t)}} = \frac{3}{[R_2^3 - R_1^3]} \frac{2}{\pi} \int_{R_1}^{R_2} \int_0^{\pi/2} \omega(R,\theta,t)\, R^2\, d\theta\, dR \qquad (22)$$

$$\overline{\overline{|\omega(t)|}} = \frac{3}{[R_2^3 - R_1^3]} \frac{2}{\pi} \int_{R_1}^{R_2} \int_0^{\pi/2} |\omega(R,\theta,t)|\, R^2\, d\theta\, dR \qquad (23)$$

$$\overline{\overline{\omega(t)^2}} = \frac{3}{[R_2^3 - R_1^3]} \frac{2}{\pi} \int_{R_1}^{R_2} \int_0^{\pi/2} \omega^2(R,\theta,t)\, R^2\, d\theta\, dR \qquad (24)$$

where the overbars denote integration over the mixing volume, and the vorticity was calculated as a finite difference approximation to the curl of the velocity field.

Figure 14 presents the evolution of the vorticity $\overline{\overline{\omega(t)}}$ averaged over the mixing region $0 \le R \le 40\ r_0$. The calculation shows that the net vorticity remains near zero. Although vorticity is baroclinically generated in positive-negative pairs that form the mushroom-capped structures seen in Figures 3-6, the net amount of vorticity remains essentially zero*.

* I.e., zero, to within a few percent of $\overline{\overline{|\omega|}}$. Nonzero values arise due to asymmetries in the vortex pairings, finite-difference errors in computing ∇ x u, and anomolies arising for the r - z form of the governing equations.

To demonstrate that vorticity is not zero everywhere, one must consider the magnitude of vorticity $\overline{|\omega|}$ or its energy $\overline{\omega^2}$. Figure 15 shows that vorticity is rapidly created and then decays. Evidently the vorticity in this calculation corresponds to a function that fluctuates about a zero mean, with the magnitude of the fluctuations decaying with time, while the kinetic energy K remains constant.

The decay of the vorticity is best illustrated by considering the enstrophy-like parameter $\varepsilon(t)$:

$$\varepsilon(t) \equiv 1/\sqrt{0.5\overline{\omega(t)^2}} \tag{25}$$

whose evolution is shown in Figure 16. Indeed, the enstrophy parameter in this calculation increases with time, and may be approximated by the linear relation:

$$\varepsilon(t) = 0.005 + 0.0345t \qquad (t > 10 \text{ ms}) \tag{26}$$

that is shown as Curve 1 in the figure. This curve has essentially the same slope as the curve derived by Batchelor[19]:

$$\varepsilon(t) = 0.134 + 0.0323t \tag{27}$$

which is shown as Curve 2 in the Figure 16. His results were based on 2-D simulations of incompressible, isotropic, homogeneous turbulence in a box, as performed by R.W. Bray. Curve 1 is also similar to our previous results for interface instabilities in high altitude explosions.

$$\varepsilon(t) = 0.15 + 0.046t \tag{28}$$

which is shown as Curve 3 in Figure 16. In reference 19, Batchelor showed that this linear growth in time was associated with a cascade process for ω^2. Although the kinetic energy was constant, $\overline{\omega^2}$ decayed as t^{-2}. He found the spectrum of ω^2 had a slope of k^{-1} in the inertial range*, and this spectrum leads to an overall decay in ω^2. Evidently there is

* Note: the corresponding slope for 3-D turbulence is $k^{-5/3}$.

also a cascade process in the present calculations. Vorticity starts at small scales, which grow with time. Additional fine-scale structures are continuously created by a folding mechanism in 2-D flows, analogous to the re-generation of fine-scale structures by hairpin vorticies in 3-D flows. This leads to a net decay in volume-average vorticity—even though the kinetic energy remains constant.

Summary and Conclusions

The fireball interface was unstable, and rapidly evolved into a convective mixing layer. During the blast wave phase the mixing width grew linearly with time $\delta/r_0 = 0.396\ t$, while during the implosion phase it grew with a power-law function of time $\delta/r_0 = 0.151\ t^{1.44}$ as a result of the inward stretching of the interface by the implosion shock. At late times it attained an asymptotically-constant width of $\delta/r_0 = 21$.

The azimuthal-averaging procedure was adequate to produce smooth, well-behaved profiles in the mixing layer. The profiles scale with the mixing layer thickness (i.e., with $\eta = (R-R_{0.5})/\delta$); in many cases the profiles were self-similar (i.e., independent of time).

The mean kinetic energy of the blast wave rapidly decayed to zero, but the fluctuating kinetic energy approached a constant (about 3.5 percent of K_{max}) at late times. This small residual value represents the rotational energy associated with turbulent mixing, and is driven by the vorticity field. Viscosity—either physical or numerical—is required to dissipate this small residual energy.

Vorticity is rapidly generated by baroclinic effects, and then evolves through a cascade process by convective mixing. For example, vorticity is created at fine scales that grow to larger and larger scales by vortex merging. At the same time, fine-scale structures are regenerated in 2-D by stretching of material lines, whereby vorticity gradients are amplified by velocity gradients[20] (similar to vertex-line stretching in 3-D flows). This leads to a vorticity distribution with the following properties:

1. The vorticity function oscillates between positive and negative values, such that the net vorticity is zero (i.e., $\overline{\overline{\omega(t)}} = 0$).

[20] Vuillermoz, P. and Oran, E.S. (1992) "Mixing Regimes in a Spatially-Confined, Two-Dimensional, Supersonic Shear Layer," (submitted to *Phys. of Fluids).*

2. A cascade process is established that causes the spectrum of ω^2 to have a slope of minus one in the inertial subrange in wave-number space[19].
3. The cascade process causes the magnitude of vorticity to decay such that $\overline{\overline{\omega(t)^2}} \approx t^{-2}$, while the corresponding enstrophy parameter grew linearly with time: $\varepsilon(t) = 0.005 + 0.0345\ t$.
4. The evolution of the vorticity was constrained such that the kinetic energy remained constant.

These results are in agreement with other 2-D simulations of turbulent mixing for incompressible flows[19] and compressible shear layers[20].

The HE-driven blast wave problem considered here provides an opportunity for investigating a variety of fluid-mechanic effects related to interface instabilities in spherical geometry. Initially the interface is accelerated impulsively as the detonation wave breaks out of the charge and instabilities grow by the Richtmyer-Meshkov mechanism during the blast wave phase. During the implosion phase, the mixing layer is drawn back toward the origin, and the mixing structures resemble those found in imploding spherical shells. During the re-shocking phase, the secondary shock S' interacts with the density structures in the fireball thus generating additional fine-scale structures by the baroclinic mechanism. What remains after shock S' leaves the fireball is a vorticity distribution that evolves according to convective mixing dynamics. This can be used to study the decay of turbulence in spherical mixing layers to arbitrarily late times.

Turbulence is, or course, a three-dimensional (3-D) phenomenon. We plan to recalculate this problem in 3-D to study the evolution of turbulence in spherical mixing layers. In addition, more detailed experimental data (e.g., Laser-Doppler-Velocimetry measurements of the velocity fluctuations, etc.) are needed to check the accuracy of the numerical simulations.

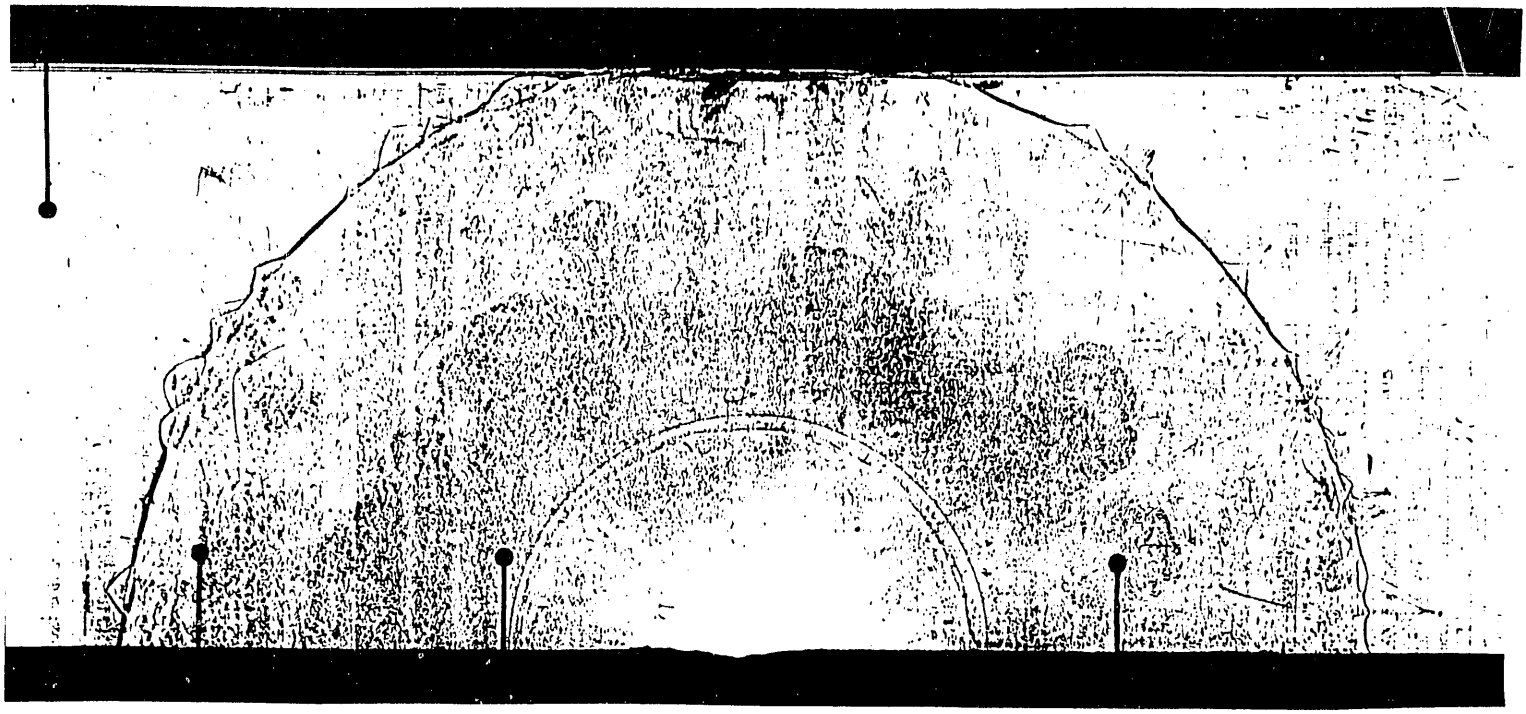

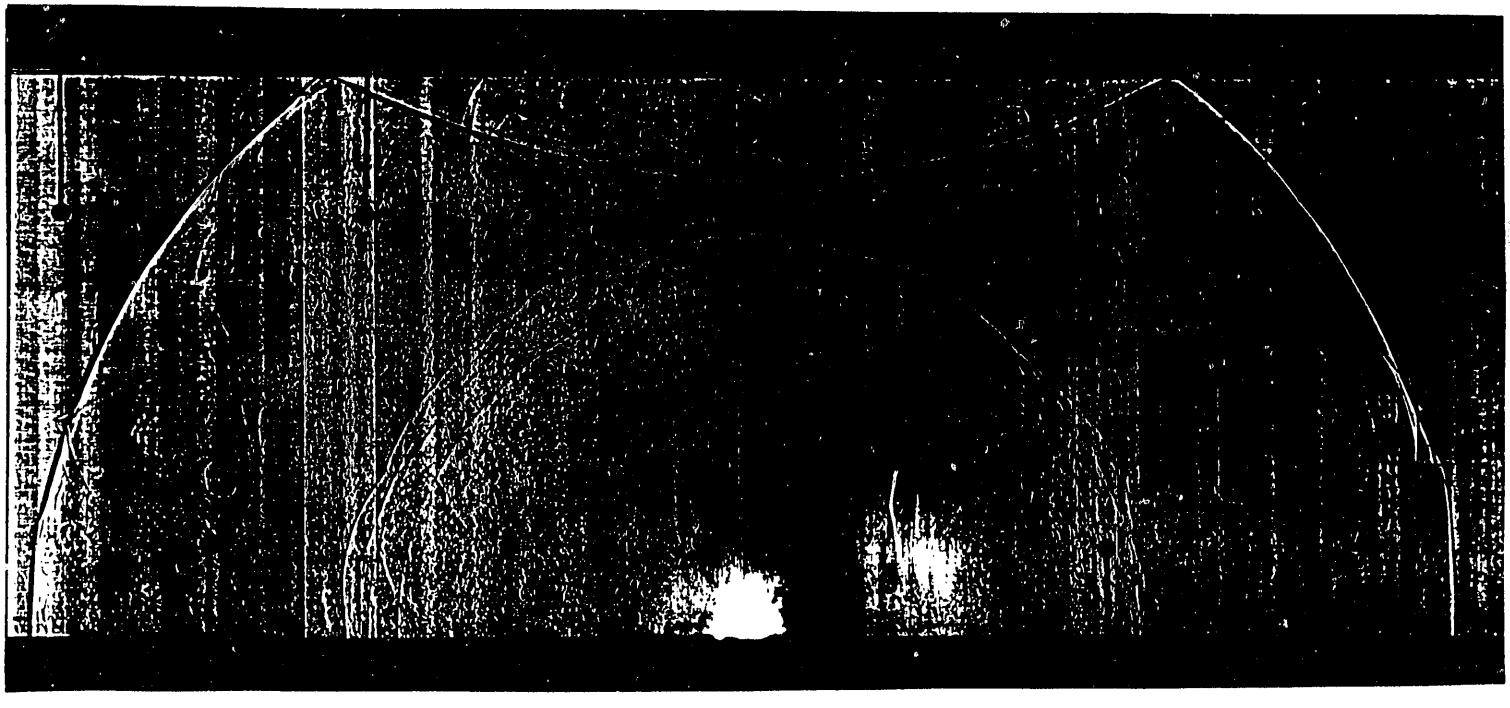

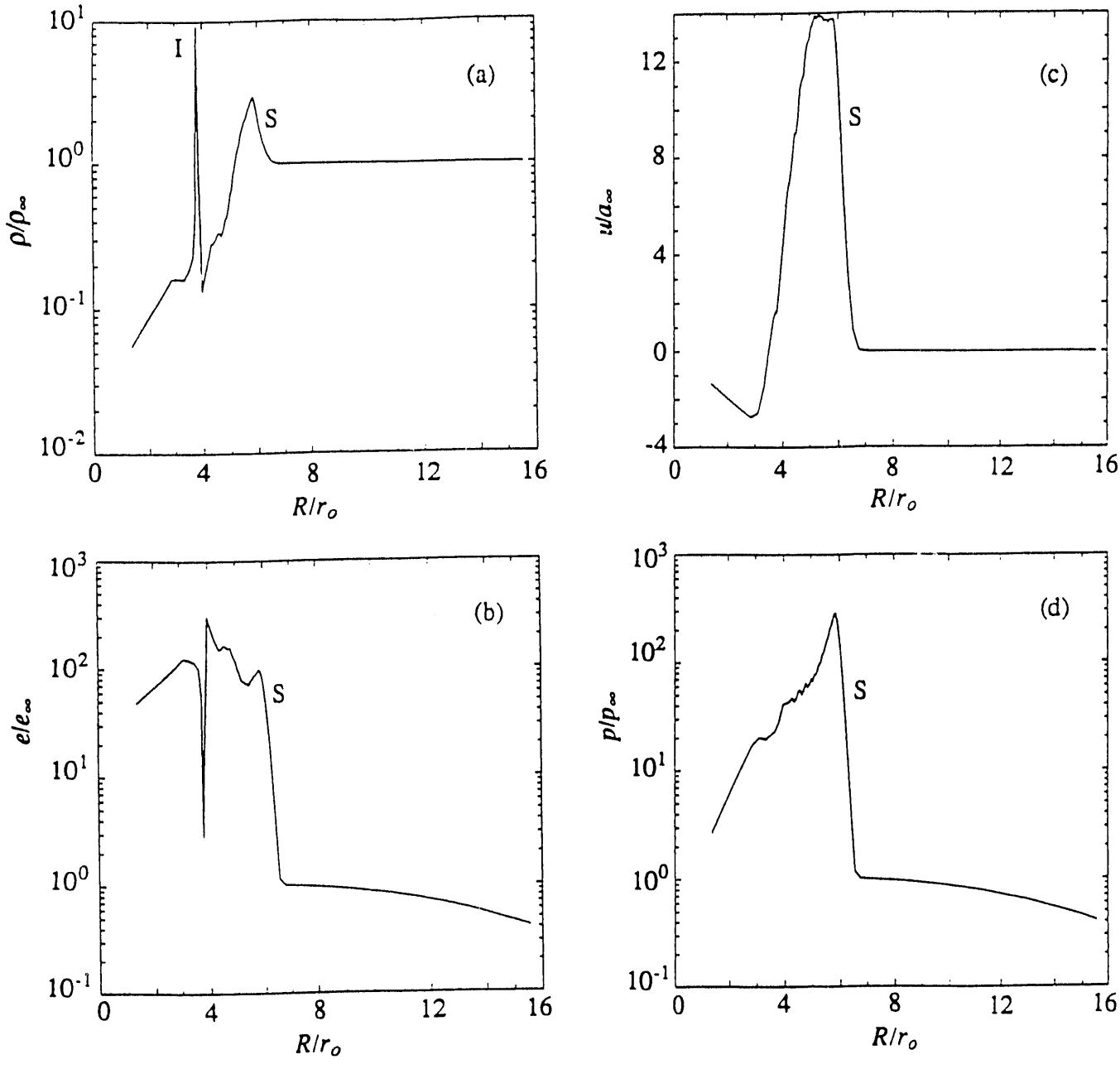

Figure 2. Initial conditions of the blast wave: (a) density; (b) internal energy; (c) radial velocity; (d) pressure.

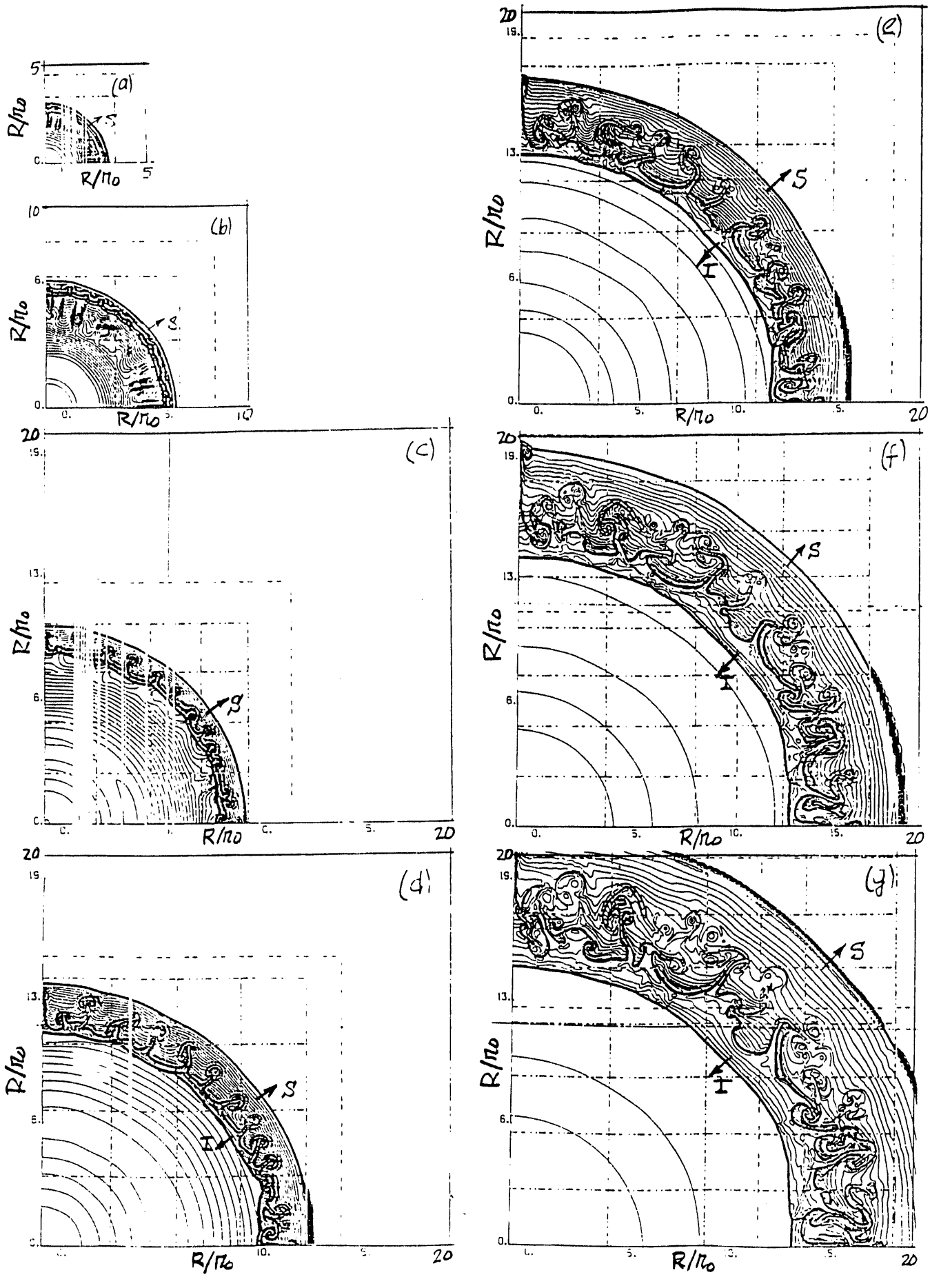

Figure 3. Growth of instabilities on the fireball interface during the blast wave expansion phase (log ρ contours): (a) t = 0.31 ma (b) t = 1.1 ms; (c) t = 2.4 ms; (d) t = 3.9 ms; (e) t = 5.8 ms; (f) t = 7.8 ms; (g) t = 9.8 ms.

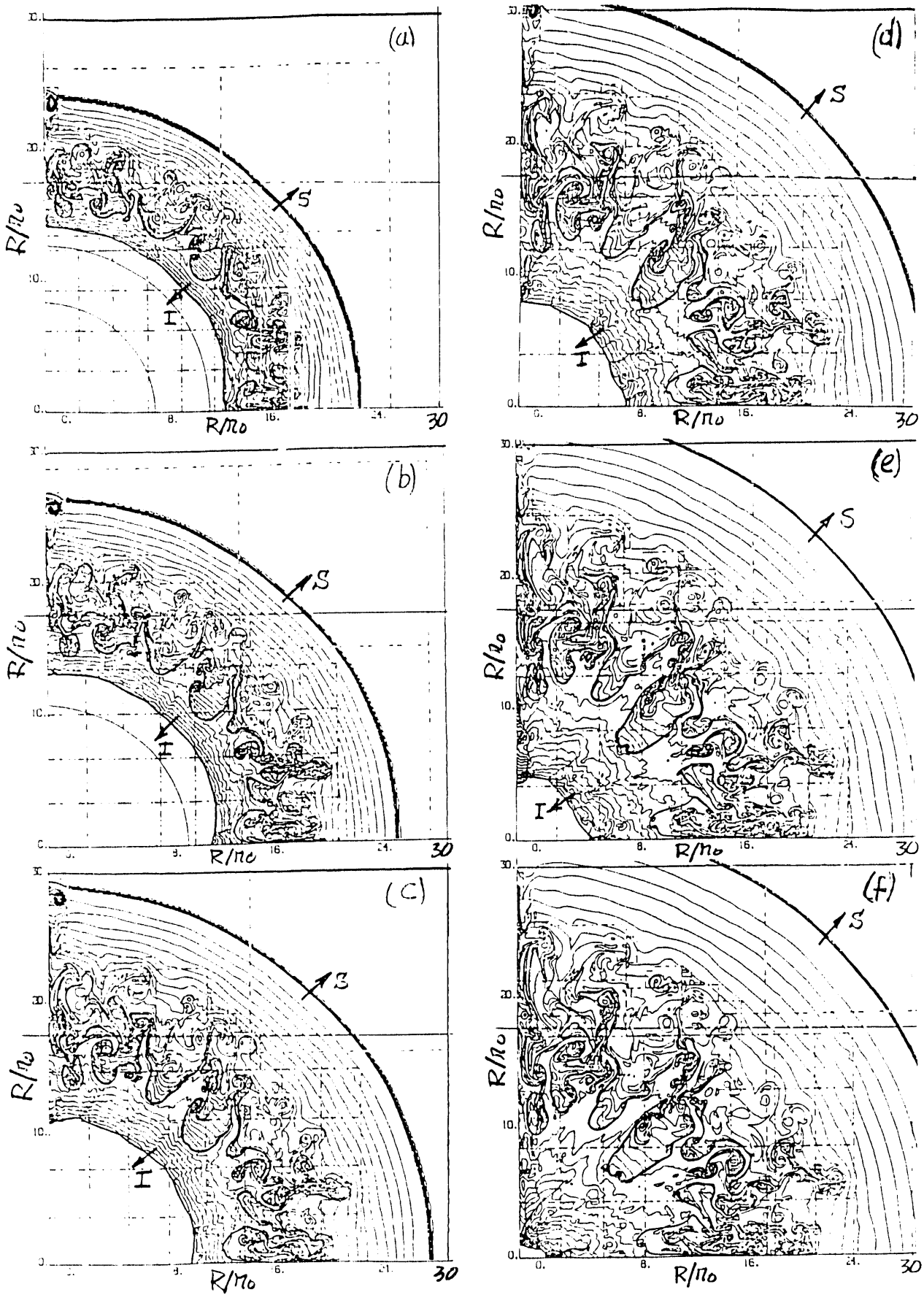

Figure 4. Growth and inward stretching of the mixing region during the implosion phase (log ρ contours): (a) t = 12.0 ms (b) t = 14.5 ms; (c) t = 17.3 ms; (d) t = 20.3 ms; (e) t = 22.1 ms; (f) t = 23.8 ms.

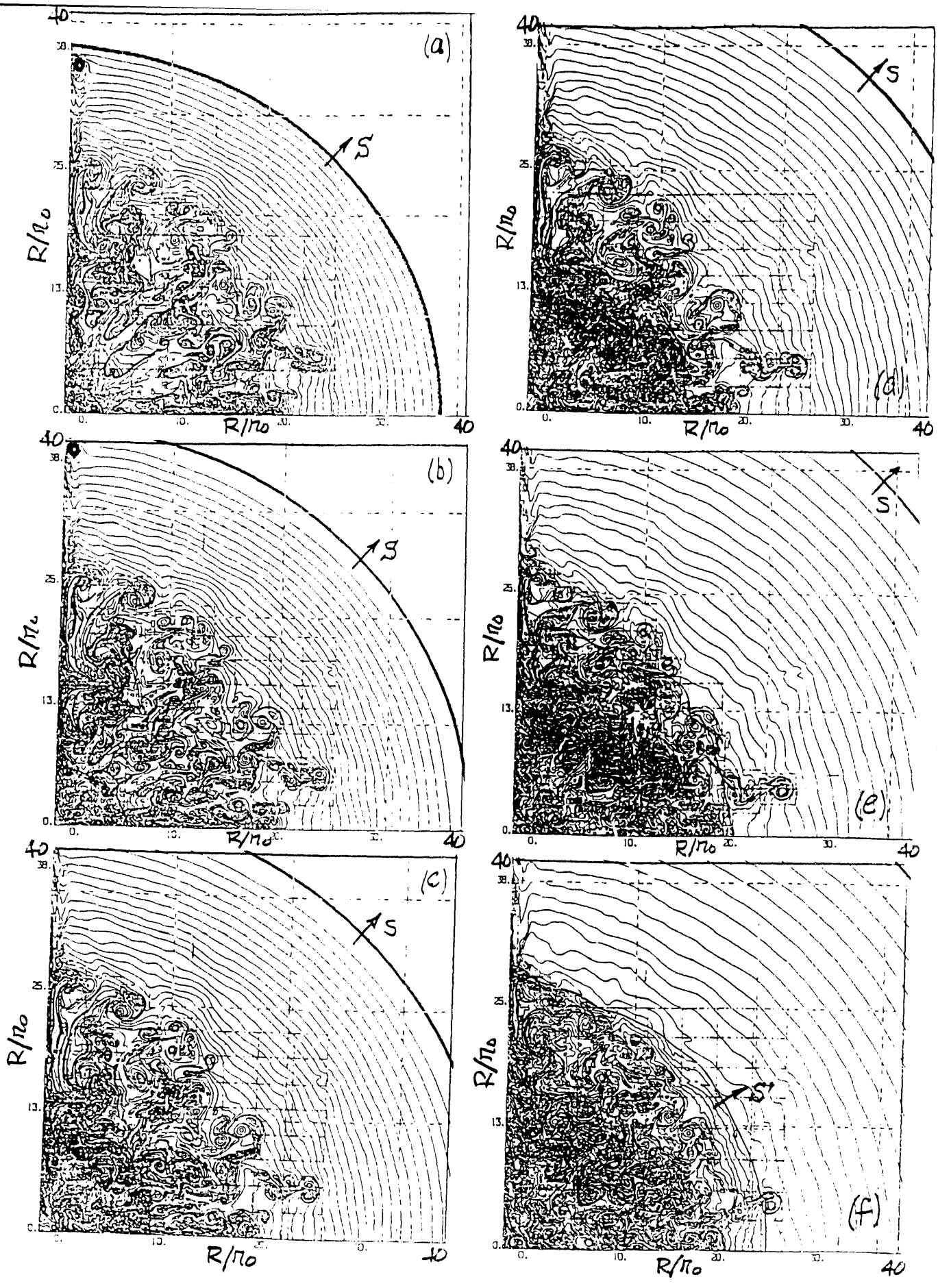

Figure 5. Evolution of mixing in the fireball during the reshocking phase (log ρ contours): (a) t = 29.2 ms; (b) t = 34.6 ms; (c) t = 40.6 ms; (d) t = 47.5 ms; (e) t = 55.1 ms; (f) t = 63.2 ms.

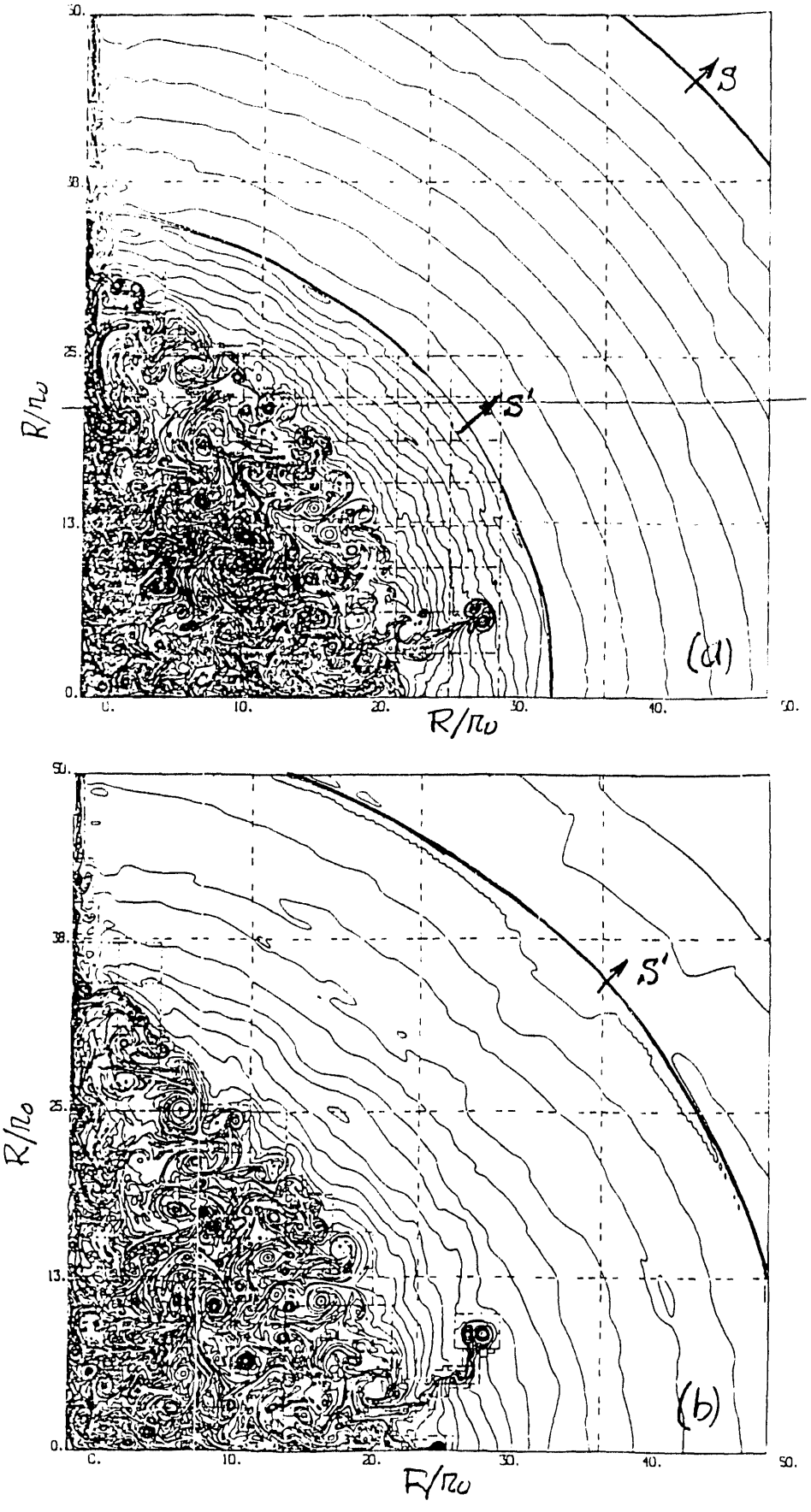

Figure 6. Mixing in the fireball during the asymptotic mixing phase (log ρ contours): (a) t = 79.1 ms; (b) t = 125.8 ms.

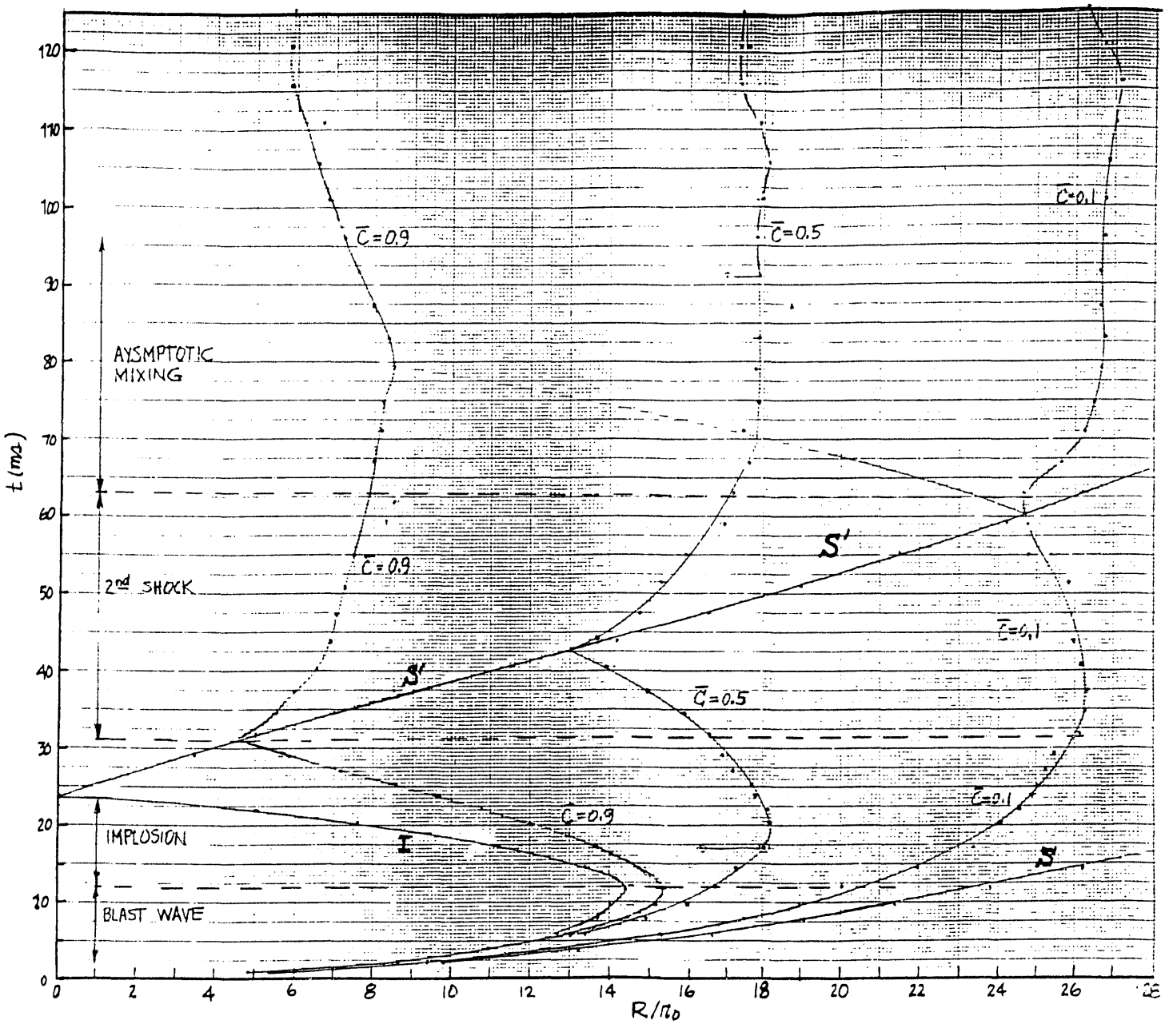

Figure 7. Wave [redacted] diagram for a HE-driven blast wave.

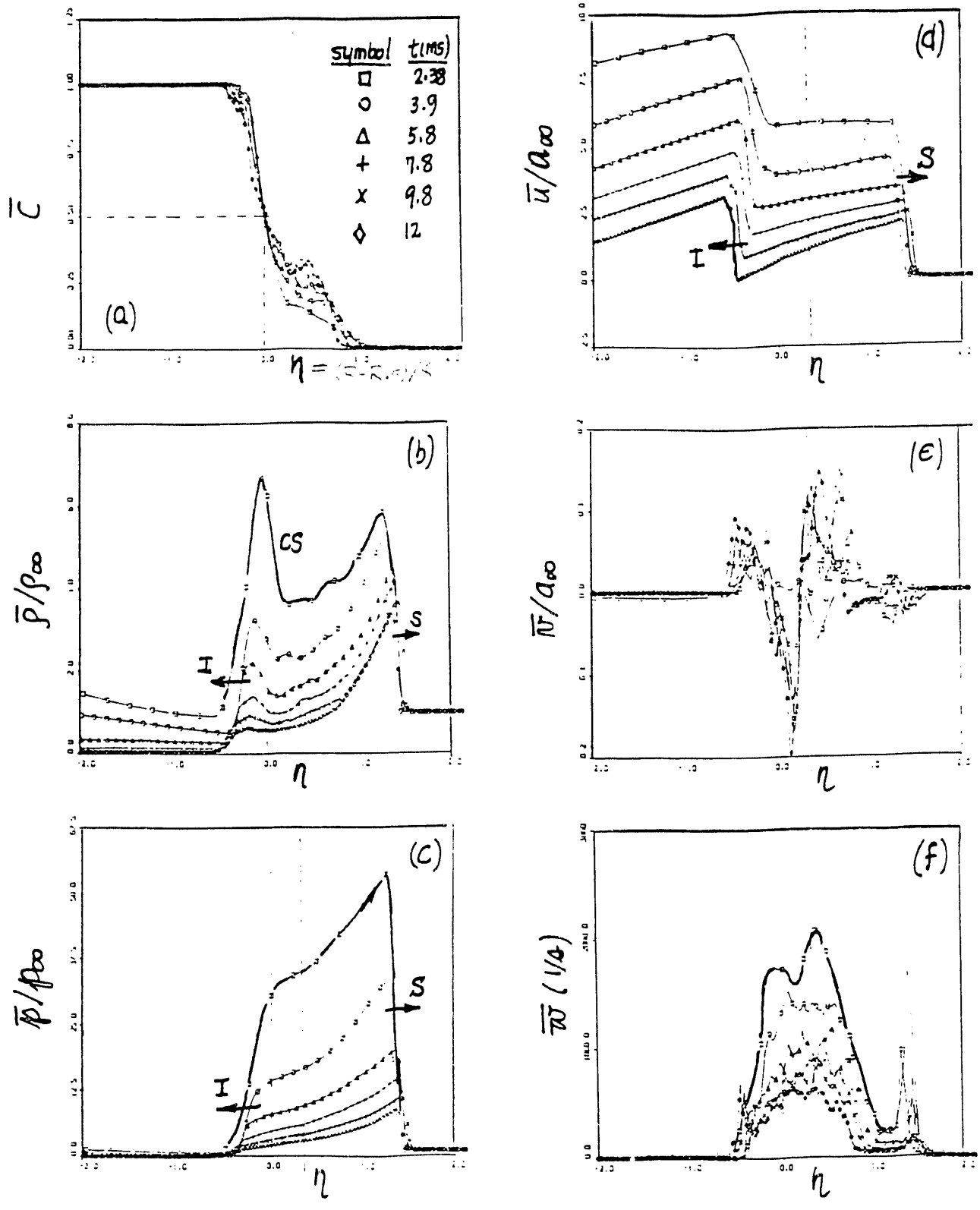

Figure 9. Azimuthally-averaged mean flow profiles during the blast wave expansion phase (2.4 ms $\leq t \leq$ 12.0 ms): (a) concentration; (b) density; (c) pressure; (d) radial velocity; (e) azimuthal velocity; (f) vorticity.

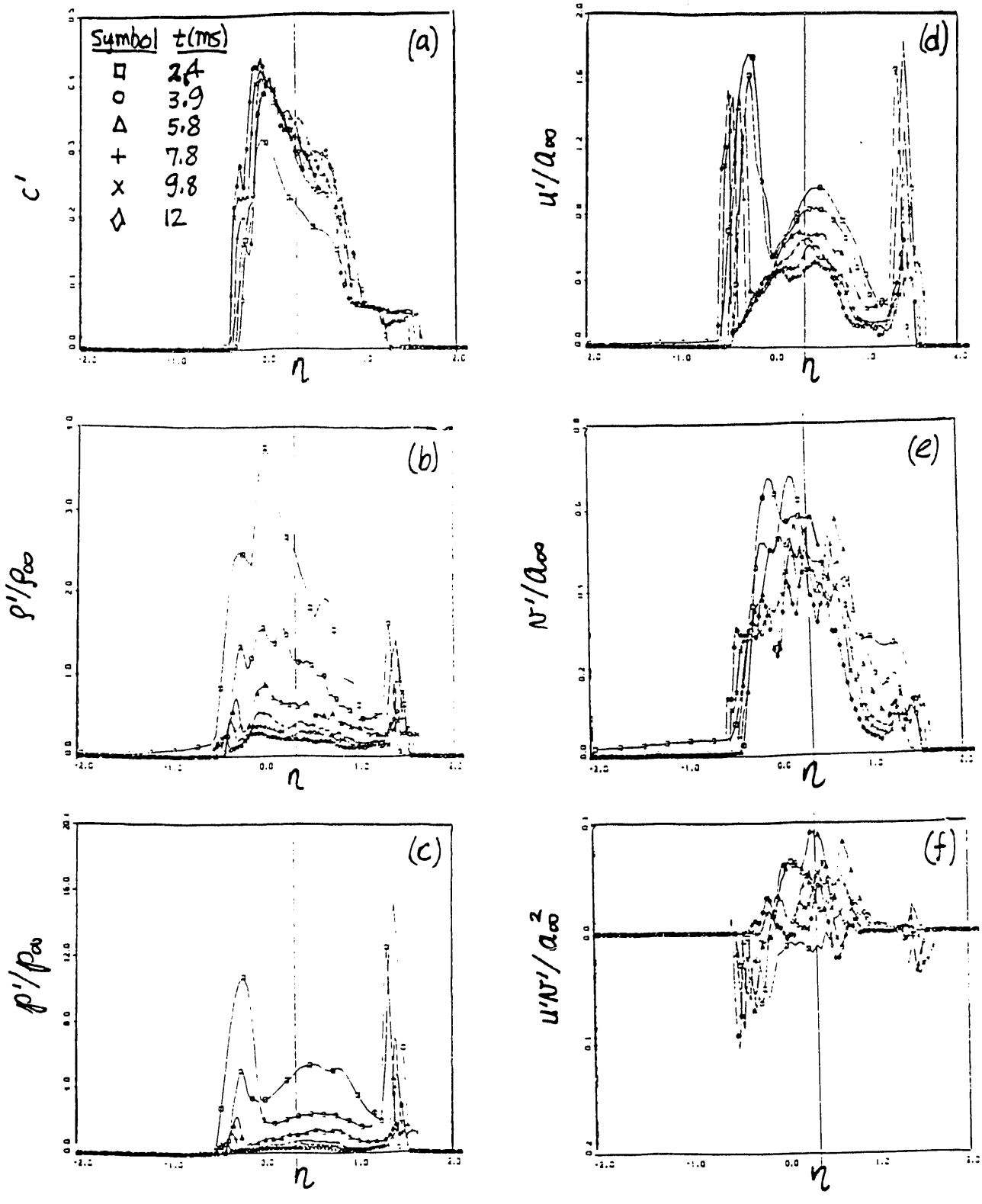

Figure 10. Azimuthally-averaged r.m.s. fluctuation profiles during the blast wave expansion phase (2.4 ms $\leq t \leq$ 12.0 ms): (a) concentration; (b) density; (c) pressure; (d) radial velocity; (e) azimuthal velocity; (f) Reynolds stress

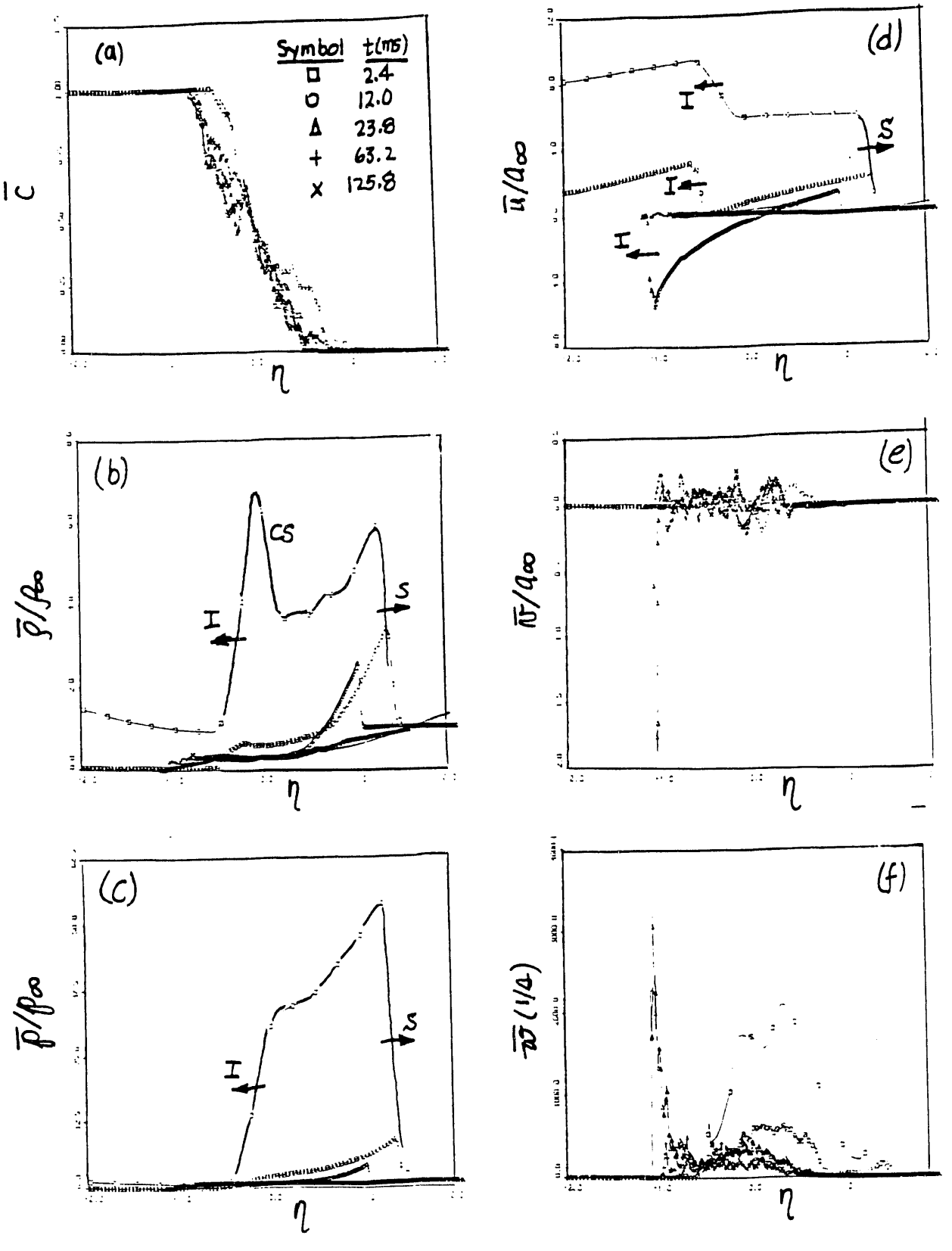

Figure 11. Evolution of the mean-flow profiles in the mixing region: (a) concentration; (b) density; (c) pressure; (d) radial velocity; (e) azimuthal velocity; (f) vorticity.

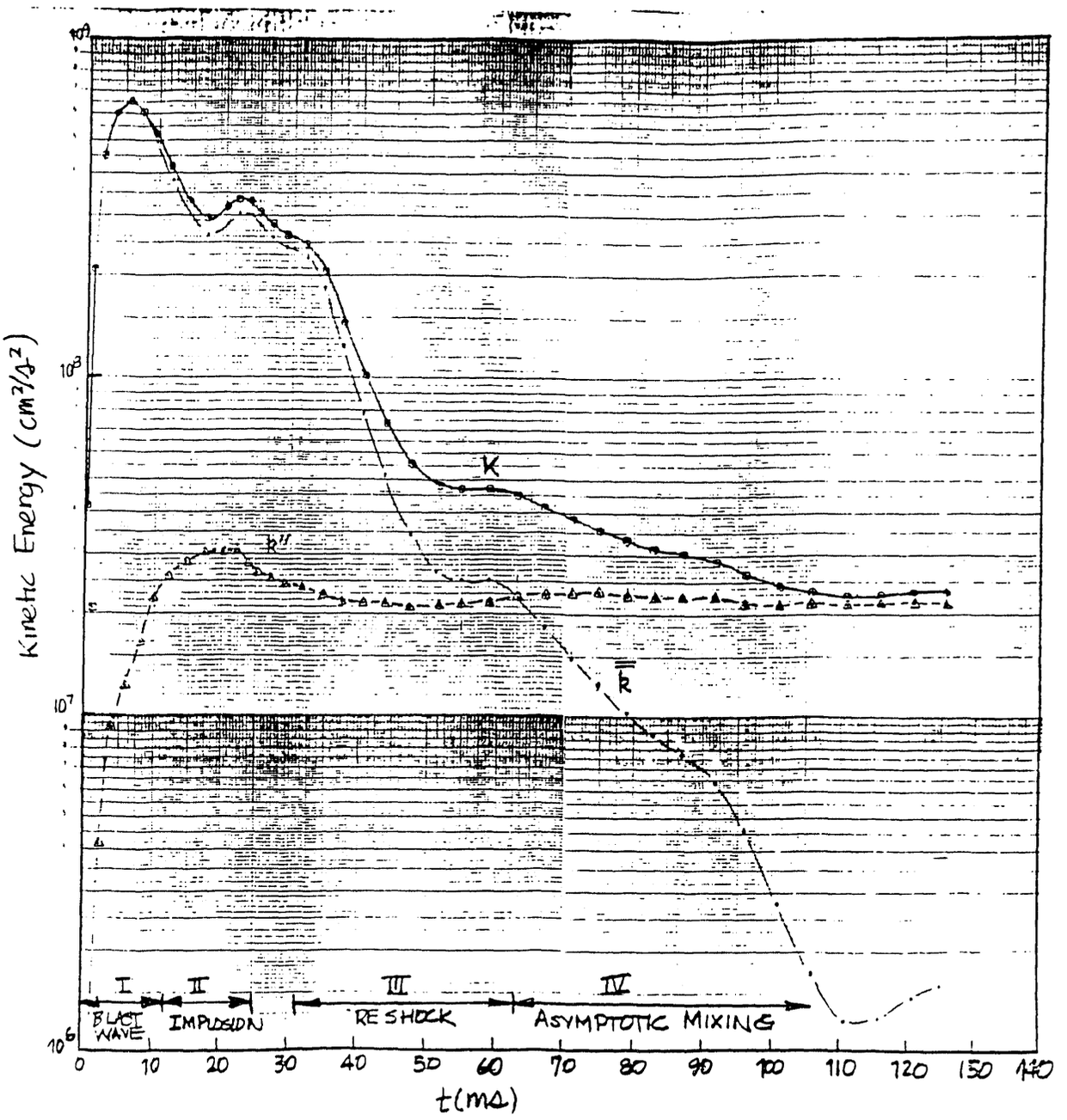

Figure 13. Evolution of the kinetic energy in the region $R \leq 40\ r_o$: mean component $\bar{\bar{k}}$, fluctuating component k", and total $K = \bar{\bar{k}} + k''$.

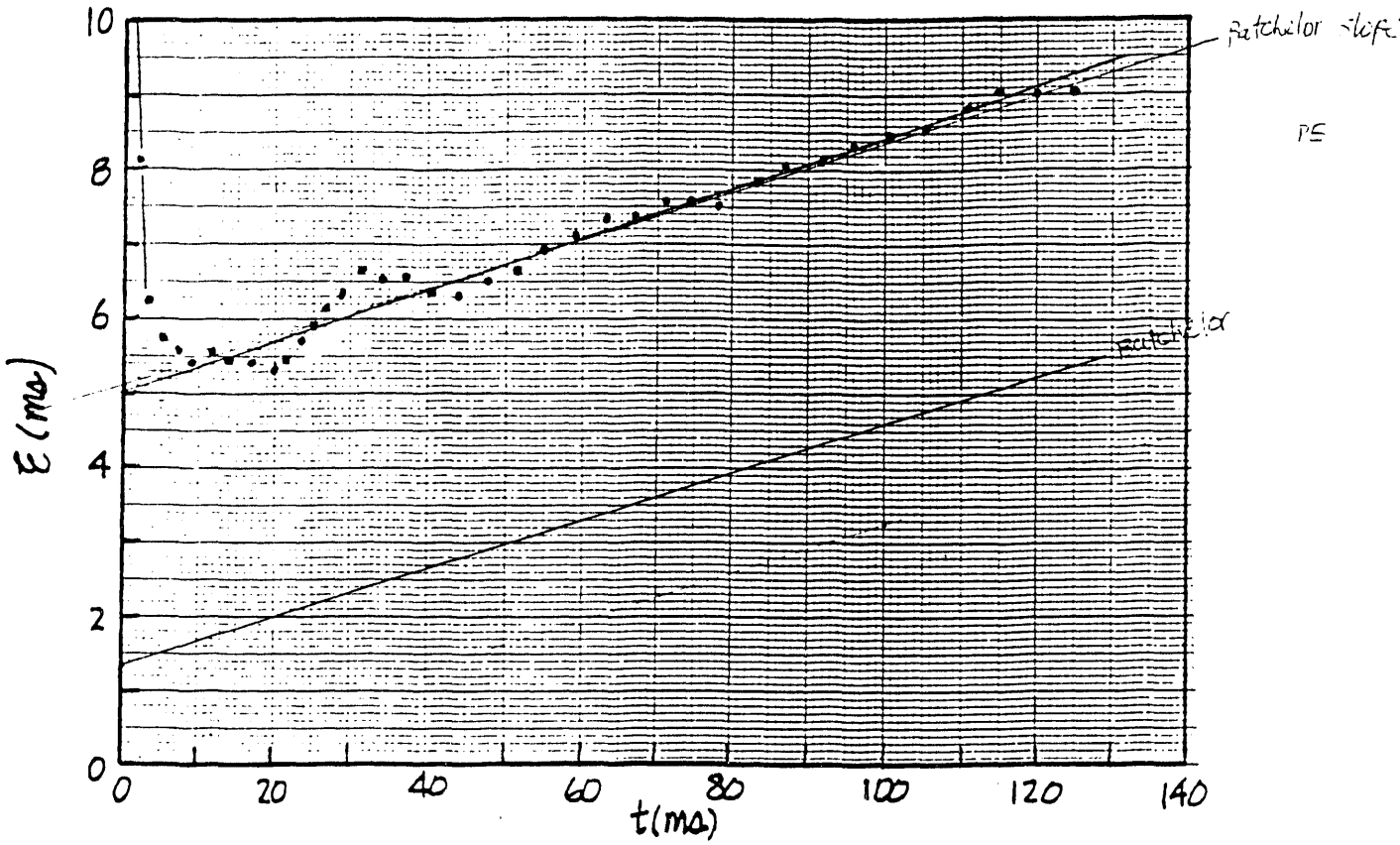

16.

Figure ~~14~~. Evolution of the Enstrophy ε in the mixing region. Data points denote the present calculation and their fit: $\varepsilon(t) = 0.005 + 0.0345\ t$.

DATE
FILMED
12/28/93
END